PHYSICAL REVIEW B **70**, 100502(R) (2004)

Flux flow and pinning of the vortex sheet structure in a two-component superconductor

Yasushi Matsunaga, Masanori Ichioka,* and Kazushige Machida
Department of Physics, Okayama University, Okayama 700-8530, Japan
(Received 4 August 2004; published 20 September 2004)

A simulation study using the time-dependent Ginzburg-Landau theory is performed for the vortex state in two-component superconductors, such as $PrOs_4Sb_{12}$. We investigate the flux flow and the pinning of the vortex sheet structure. We find a domain wall that traps half flux-quantum vortices and moves with the flux flow. In the pinning case, we observe an emitting process of a conventional vortex from the vortex sheet by combining a pair of half flux-quantum vortices.

DOI: 10.1103/PhysRevB.70.100502 PACS number(s): 74.25.Qt, 74.20.Rp, 74.20.De, 74.70.Tx

Some exotic unconventional superconductors have multiple superconducting phases, indicating a multicomponent pair potential of the superconductivity. In these superconductors, we expect interesting behavior to occur through a combination of the multiple components.

In the superconductor $PrOs_4Sb_{12}$, which is a heavy fermion compound with a filled skutterdite structure, thermal conductivity experiments have shown a multiple superconducting phase diagram with two phases, the *A* (in the higher *H* region) and *B* (lower *H*) phases.[1] Multicomponent superconductivity is also suggested by the spontaneous moment in the superconducting phase reported in muon spin relaxation (μSR) experiments.[2] As an another example, UPt_3 has a double transition of superconductivity and the superconducting phase is divided into three phases, indicating multicomponent superconductivity.[3–7]

Considering the two component case for simplicity, the pair potential in a 2×2 matrix form can be decomposed as $\hat{\Delta}(\mathbf{r},\mathbf{k})=\eta_1(\mathbf{r})\hat{\phi}_1(\mathbf{k})+\eta_2(\mathbf{r})\hat{\phi}_2(\mathbf{k})$ with the order parameter $\eta_m(\mathbf{r})$, where $\mathbf{r}$ is the center-of-mass coordinate of the Cooper pair and $m=1,2$. The pairing function, depending on the relative momentum $\mathbf{k}$ of the pair, is given by $\hat{\phi}_m(\mathbf{k})=i\hat{\sigma}_y\phi_m(\mathbf{k})$ for the spin singlet pairing, and $\hat{\phi}_m(\mathbf{k})=i\Sigma_{j=x,y,z}\, d_{m,j}(\mathbf{k})\hat{\sigma}_j\hat{\sigma}_y$ for the triplet pairing with Pauli matrices $\hat{\sigma}_x$, $\hat{\sigma}_y$, and $\hat{\sigma}_z$. In the double transition of superconductivity, after the first component η_1 appears at the first transition, the second component η_2 appears at the second transition.[8,9] We discuss in this paper the exotic vortex structure due to the combination of the two components below the second transition.

Superfluidity of ^{3}He, which has *A* and *B* phases, is also a typical example of multicomponent pair potentials. Chiral *p*-wave superconductivity in Sr_2RuO_4 should be treated as a two-component superconductor with k_x+ik_y-wave and k_x-ik_y-wave components, or k_x-wave and k_y-wave components, when we consider the vortex,[10–12] the domain wall, and boundary states.[13]

In multicomponent superconductors, some superconducting states are degenerate in free energy. In a simple example of weak-coupling singlet pairing with $\phi_1=\phi_A$ and $\phi_2=i\phi_B$, two states $\Delta_\pm=\eta_1\phi_A\pm i\eta_2\phi_B$ are degenerate when $|\Delta_+|=|\Delta_-|$. Therefore, a domain structure may appear in a multicomponent superconductor, i.e., some regions in a sample are a Δ_+ domain and others are a Δ_- domain. Between the domains, domain walls appear as topological defects, which are not easily destroyed.

When magnetic fields are applied to this domain structure, some of the vortices are trapped at the domain wall. The vortices at the domain wall form an exotic structure called a "vortex sheet,"[14] where a conventional vortex splits into two vortices with half flux quanta.[15–17] We confirmed the appearance of the vortex sheet by a simulation in a previous paper.[9] This interesting vortex sheet structure can be a clue to the presence of the domain wall, which would be clear evidence of unconventional multicomponent superconductors.

When a supercurrent flows in the vortex state, vortices flow in the direction transverse to the current, which is the origin of the flux flow resistivity. In order to stop the vortex motion and prevent flux flow resistivity, we need to introduce pinning centers for vortices in the sample. The purpose of this paper is to investigate the dynamics of the vortex sheet structure by simulation of flux flow and pinning based on the time-dependent Ginzburg-Landau (TDGL) theory, and to examine how vortices and the domain wall of the vortex sheet structure move under the current flow in the presence of pinning centers. These dynamics may affect the flux flow resistivity or the magnetization process in multicomponent superconductors. The TDGL theory is used as a phenomenological approach in our qualitative study, with the expectation that vortices move so as to approach the free energy minimum state. Contrary to a full-gap superconductor, since unconventional superconductors have low energy quasiparticle states available for the dissipation process within the superconducting gap due to the gap node, we expect that the TDGL theory can be qualitatively applied without considering the extreme case of the dirty limit.

We start from the two-component Ginzburg-Landau (GL) theory that was used in our previous study on the double transition of $PrOs_4Sb_{12}$. The GL free energy density in the dimensionless form is written as[9]

$$\tilde{f} = -\left[\nu(\mathbf{r}) - \frac{T}{T_c}\right]|\eta_1|^2 - \left[\frac{T_{c2}}{T_c}\nu(\mathbf{r}) - \frac{T}{T_c}\right]|\eta_2|^2 + \eta_1^*(q_x^2 + q_y^2)\eta_1$$
$$+ C_{22x}\eta_2^* q_x^2 \eta_2 + C_{22y}\eta_2^* q_y^2 \eta_2 + C_{12x}\eta_1^* q_x^2 \eta_2 + C_{12x}^* \eta_2^* q_x^2 \eta_1$$
$$+ C_{12y}\eta_1^* q_y^2 \eta_2 + C_{12y}^* \eta_2^* q_y^2 \eta_1 + \frac{1}{2}\{|\eta_1|^4 + C_2|\eta_2|^4$$
$$+ 4C_3|\eta_1|^2|\eta_2|^2 + C_4^* \eta_1^{*2}\eta_2^2 + C_4 \eta_2^{*2}\eta_1^2\}, \quad (1)$$

where $\mathbf{q} = (\hbar/i)\nabla + (2\pi/\phi_0)\mathbf{A}$ with flux quantum ϕ_0 and vector potential $\mathbf{A}$, and we write $C_{22x} \equiv (1-\epsilon)/(X\sqrt{1-\epsilon^2})$ and $C_{22y} \equiv (1+\epsilon)/(X\sqrt{1-\epsilon^2})$. Inside the pinning center region, where the superconductivity is suppressed, we set $\nu(\mathbf{r}) = 0$.[18] In other regions, $\nu(\mathbf{r}) = 1$. The GL theory covers both singlet and triplet pairings and we can study the vortex states without specifying the pairing function $\hat{\phi}(\mathbf{k})$. The coefficients in Eq. (1) are related to the information of the pairing symmetry and the Fermi surface anisotropy as described in Ref. 9. However, since this information has not been established yet, we treat the coefficients as arbitrary parameters.

We consider a phase below the second transition, where both η_1 and η_2 appear. From Eq. (1), we recognize that the relative phases of η_1 and η_2 should be $(\alpha+\pi)/2$ or $(\alpha-\pi)/2$ in the free energy minimum state in a zero field, where α is given by $C_4 = |C_4|e^{i\alpha}$. These two states correspond to Δ_+ and Δ_- noted in the introduction.

For simulations of the vortex dynamics we use the TDGL equation coupled with Maxwell equations:[18–20]

$$\frac{\partial}{\partial t}\eta_1 = -\frac{1}{12}\frac{\partial \tilde{f}}{\partial \eta_1^*}, \quad \frac{\partial}{\partial t}\eta_2 = -\frac{1}{12}\frac{\partial \tilde{f}}{\partial \eta_2^*}, \quad (2)$$

$$\frac{\partial}{\partial t}\mathbf{A} = \tilde{\mathbf{j}}_s - \kappa^2 \nabla \times \mathbf{B}, \quad \mathbf{B} = \nabla \times \mathbf{A}. \quad (3)$$

The supercurrent $\tilde{\mathbf{j}}_s = (\tilde{j}_{s,x}, \tilde{j}_{s,y}) \propto (\partial\tilde{f}/\partial A_x, \partial\tilde{f}/\partial A_y)$ is given by

$$\tilde{j}_{s,x} = \mathrm{Re}[\eta_1^*(q_x\eta_1) + C_{22x}\eta_2^*(q_x\eta_2) + C_{12x}\eta_1^*(q_x\eta_2)$$
$$+ C_{12x}^*\eta_2^*(q_x\eta_1)], \quad (4)$$

$$\tilde{j}_{s,y} = \mathrm{Re}[\eta_1^*(q_y\eta_1) + C_{22y}\eta_2^*(q_y\eta_2) + C_{12y}\eta_1^*(q_y\eta_2)$$
$$+ C_{12y}^*\eta_2^*(q_y\eta_1)]. \quad (5)$$

The length, field, and time are, respectively, scaled by the coherence length ξ_0, $H_{c2,0} = \phi_0/2\pi\xi_0^2$, and $t_0 = 4\pi\xi_0^2\kappa^2\sigma/c^2$ with the normal state conductivity σ.[18–20] However, we here scale η_m by η_0 instead of $\eta_0(T) = \eta_0(1-T/T_c)^{1/2}$. η_0 is a uniform solution of η_1 when $\eta_2 = 0$, $\nu(\mathbf{r}) = 1$, and $T = 0$. The calculations are performed in a two-dimensional square area with each side of length of W and a current flow j, as schematically shown in Fig. 1. Outside the open boundary we set $\eta_1 = \eta_2 = 0$, and at the lower and upper boundaries we set $B(\mathbf{r}) = H_+$ and H_-, respectively, where $H_\pm = H_0 \pm Wj/2$ for an applied field H_0.[20]

We report the case when the gradient coupling is absent ($C_{12x} = C_{12y} = 0$).[21] We set $T_{c2}/T_c = 0.9$, $\kappa = 4$, $C_2 = 1$, $C_3 = -C_4 = 0.2$, $\epsilon = 0$, and $X = 0.5$. If C_4 is negative (i.e., $\alpha = \pi$),

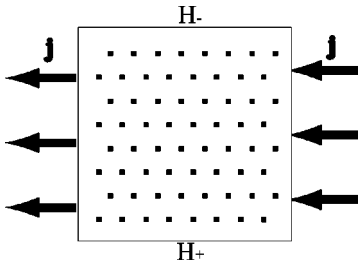

FIG. 1. Configuration of the simulation. The current density j flows in at the right-hand side boundary and out at the left-hand side boundary of $W \times W$ square superconductors. External fields H_+ and H_- are applied outside the lower and upper boundaries, respectively. For the pinning case, we introduce pinning centers where the superconductivity is suppressed, represented by small solid squares.

then $\phi_1 = \phi_A$ and $\phi_2 = i\phi_B$, if the pairing is a singlet. We note that our results for the vortex sheet do not significantly depend on the selection of the coefficients in Eq. (1), because the appearance of the domain wall only results from two states with the relative phase $(\alpha \pm \pi)/2$ being degenerate in free energy. We report results for $T = 0.1T_c$, $H = 0.2H_{c2,0}$, $j = 2.6 \times 10^{-3}$, and $W = 57\xi_0$ as a typical example. In this simulation, we start from a uniform initial state with relative phase 0, and switch on H_0 and j at $t = 0$.

In some cases of the penetration process of vortices, vortex sheet structures are created at the boundary and move toward the inside.[9] On the other hand, the vortex sheet can be produced if we apply a magnetic field after preparing the domain wall at a zero field. In this case, some penetrating vortices are trapped at the domain wall and these trapped vortices become a vortex sheet by splitting into half flux-quantum vortices.

First, we study the free flux flow case without pinning centers, as shown in Fig. 2.[22] The left panels show a color map of the spatial distribution of $|\eta_1(\mathbf{r})|$ and $|\eta_2(\mathbf{r})|$. The black circle region shows a conventional vortex with a flux quantum, where $|\eta_1(\mathbf{r})|$ and $|\eta_2(\mathbf{r})|$ share the same vortex core. The green and red circle regions show the η_1 and η_2 vortices, respectively, where only $|\eta_1(\mathbf{r})|$ or $|\eta_2(\mathbf{r})|$, respectively, has a vortex core and the other, $|\eta_2(\mathbf{r})|$ or $|\eta_1(\mathbf{r})|$, does not. These green and red vortex cores are located alternatively along a loop, forming a vortex sheet. The area including both an η_1 vortex and an η_2 vortex is equal to that of a conventional vortex, indicating that each of the two vortices η_1 and η_2 has half flux quanta. The right panels show the relative phase $\arg\{\eta_1(\mathbf{r})/\eta_2(\mathbf{r})\}$, where we recognize that the vortex sheet is along the domain wall between the domains of relative phase π (blue region) and relative phase 0 (red region). The relative phase has a phase winding 2π or -2π around the η_1 or η_2 vortex, respectively. In this free flux flow case, a conventional vortex flows upward, i.e., in a perpendicular direction to the current. The vortex sheet structure also simply flows with the same flow as conventional vortices. That is, the domain wall moves with the trapping half flux-quantum vortices under current flow. The half flux-quantum vortices rarely escape from the domain wall of the vortex sheet in this free flux flow case.

To study dynamical processes involving the vortex sheet and conventional vortices in a complicated manner, we intro-

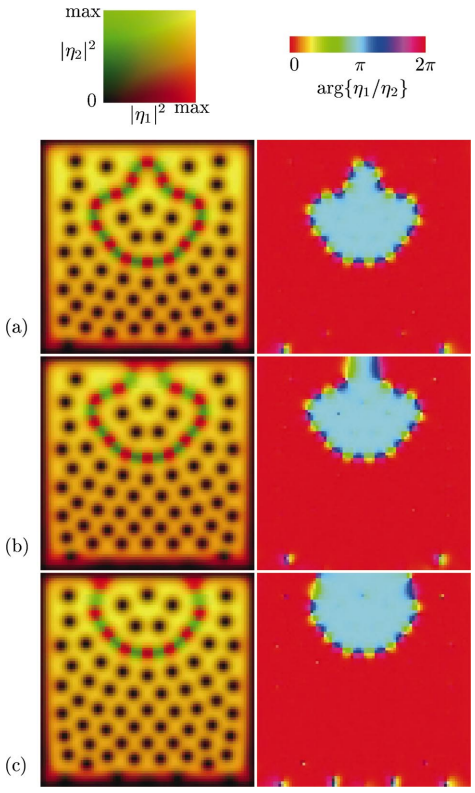

FIG. 2. (Color) Time evolution of the vortex state in the free flux flow case without pinning centers. Snapshots of the total $W \times W$ area are presented for (a) $t/54t_0=17$, (b) 22, and (c) 27. The left panels show color density plots of $|\eta_1(\mathbf{r})|$ and $|\eta_2(\mathbf{r})|$. The black region is the core of the conventional vortex. The green and red regions are the cores of the η_1 and η_2 vortices, respectively, along the vortex sheet. The right panels show the relative phase $\arg\{\eta_1(\mathbf{r})/\eta_2(\mathbf{r})\}$. The red and blue regions are the domains of relative phase 0 and π, respectively.

duce pinning centers to prevent the flux flow. Figure 3 shows the time evolution of the flux flow states in the presence of pinning,[22] where pinning centers with a $1.4\xi_0 \times 1.4\xi_0$ square area are introduced periodically, as presented in Fig. 1. Vortices move slowly, repeatedly being trapped at pinning centers and escaping from them. The line of the vortex sheet also moves slowly and meanders due to the trapping of η_1 and η_2 vortices by the pinning centers. Compared with the slow motion of a conventional vortex and the line of the vortex sheet, η_1 and η_2 vortices easily flow along the domain wall of the vortex sheet, as indicated by arrows in Fig. 3(b). It seems that the barrier for escaping from a pinning center is lower along the line of the vortex sheet, because the vortex sheet is incommensurate with the pinning centers and the intervortex distance is short in this direction. Therefore, in the pinning case the domain wall forms a "channel" through which the vortex can flow. When the domain wall is connected to the sample boundary, vortices penetrate into the sample through the domain wall channel. These half flux-quantum vortices, quickly moving through the channel, are emitted from the vortex sheet at the front corner of the slowly moving vortex sheet line. At the emitting point, pairs of half flux-quantum vortices combine to become a conventional vortex and the created conventional vortex is released from the domain wall of the vortex sheet.

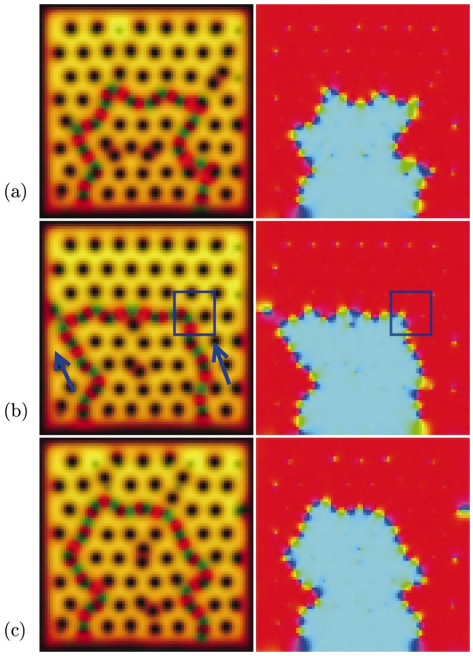

FIG. 3. (Color) Time evolution of the vortex state in the presence of pinning centers. Snapshots are presented for (a) $t/54t_0=196$, (b) 276, and (c) 356. The left panels show color density plots of $|\eta_1(\mathbf{r})|$ and $|\eta_2(\mathbf{r})|$. The right panels show the relative phase $\arg\{\eta_1(\mathbf{r})/\eta_2(\mathbf{r})\}$.

Figure 4 shows the time evolution of this emitting process in an enclosed region in Fig. 3(b). In the upper panel in Fig. 4(a) we see that vortices are trapped around pinning centers, represented by purple square regions. In the lower panels in Fig. 4, we find vortex centers of η_1 or η_2 vortices as winding centers of the relative phase (between the yellow and purple regions). In Fig. 4(a), η_1 and η_2 vortices flow upward along the vortex sheet line. However, the vortex sheet cannot easily move because some of the η_1 and η_2 vortices in the vortex

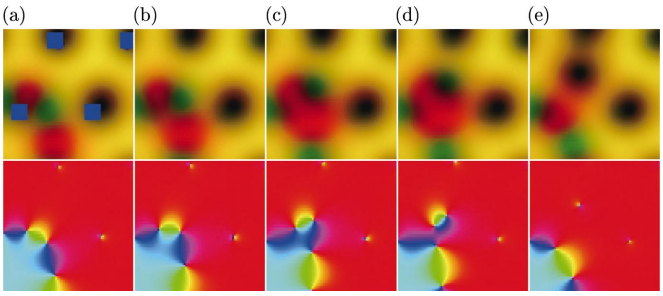

FIG. 4. (Color) Time evolution of the creation of a conventional vortex from half flux-quantum vortices in the vortex sheet. Snapshots at (a) $t/54t_0=276$, (b) 284, (c) 290, (d) 292, and (e) 296 are presented within the enclosed area shown in Fig. 3(b). The upper panels show color density plots of $|\eta_1(\mathbf{r})|$ and $|\eta_2(\mathbf{r})|$. The positions of the pinning centers are represented by purple squares in (a). The lower panels show the relative phase $\arg\{\eta_1(\mathbf{r})/\eta_2(\mathbf{r})\}$. The winding center between the yellow and purple regions is a vortex center of η_1 or η_2 vortices.

sheet are trapped by pinning centers. Therefore, near the front corner of the domain wall shown in Fig. 4, the intervortex distance of η_1 and η_2 vortices becomes short and the curvature of the domain wall becomes sharp [(a)→(b)→(c)]. This deformation of the domain wall shape helps the creation of the conventional vortex. After the core region of two η_2 vortices (the red regions in the upper panels) overlap, one of the η_2 vortices forms a pair with a neighbor η_1 vortex [(c)→(d)]. This η_1 and η_2 vortex pair combines to become a conventional vortex (the black region) and leaves the domain wall [(e)]. We also observe the inverse process where a conventional vortex is trapped to the vortex sheet and changes to a pair of η_1 and η_2 vortices in the pinning case simulation. This event is rare, but occasionally observed.

In summary, we have performed a TDGL simulation for the flux flow and the pinning in a two-component superconductor, and investigated the dynamics of the domain wall and half flux-quantum vortices of the vortex sheet structure. The domain wall moves with the flux flow both in the free flux flow case and the pinning case. We succeeded in observing the creation process wherein a pair of half flux-quantum vortices is changed to a conventional vortex and released from the vortex sheet. Relating these phenomena, the vortex sheet structure may contribute to the flux flow resistivity or the magnetization process in multicomponent superconductors, such as in $PrOs_4Sb_{12}$, UPt_3, and Sr_2RuO_4. A quantitative estimate of these interesting contributions is left for future studies.

*Electronic address: oka@mp.okayama-u.ac.jp

[1] K. Izawa, Y. Nakajima, J. Goryo, Y. Matsuda, S. Osaki, H. Sugawara, H. Sato, P. Thalmeier, and K. Maki, Phys. Rev. Lett. **90**, 117001 (2003).
[2] Y. Aoki, A. Tsuchiya, T. Kanayama, S. R. Saha, H. Sugawara, H. Sato, W. Higemoto, A. Koda, K. Ohishi, K. Nishiyama, and R. Kadono, Phys. Rev. Lett. **91**, 067003 (2003).
[3] S. Adenwalla, S. W. Lin, Q. Z. Ran, Z. Zhao, J. B. Ketterson, J. A. Sauls, L. Taillefer, D. G. Hinks, M. Levy, and B. K. Sarma, Phys. Rev. Lett. **65**, 2298 (1990).
[4] G. Bruls, D. Weber, B. Wolf, P. Thalmeier, B. Lüthi, A. de Visser, and A. Menovsky, Phys. Rev. Lett. **65**, 2294 (1990).
[5] N. H. van Dijk, A. de Visser, J. J.M. Franse, S. Holtmeier, L. Taillefer, and J. Flouquet, Phys. Rev. B **48**, 1299 (1993).
[6] K. Machida, M. Ozaki, and T. Ohmi, J. Phys. Soc. Jpn. **58**, 4116 (1989).
[7] T. Fujita, W. Aoyama, K. Machida, and T. Ohmi, J. Phys. Soc. Jpn. **63**, 247 (1994).
[8] J. Goryo, Phys. Rev. B **67**, 184511 (2003).
[9] Y. Matsunaga, M. Ichioka, and K. Machida, Phys. Rev. Lett. **92**, 157001 (2004).
[10] R. Heeb and D. F. Agterberg, Phys. Rev. B **59**, 7076 (1999).
[11] M. Takigawa, M. Ichioka, K. Machida, and M. Sigrist, Phys. Rev. B **65**, 014508 (2002).
[12] M. Ichioka and K. Machida, Phys. Rev. B **65**, 224517 (2002).
[13] M. Matsumoto and M. Sigrist, J. Phys. Soc. Jpn. **68**, 994 (1999).
[14] Ü. Parts, E. V. Thuneberg, G. E. Volovik, J. H. Koivuniemi, V. M. H. Ruutu, M. Heinilä, J. M. Karimäki, and M. Krusius, Phys. Rev. Lett. **72**, 3839 (1994).
[15] M. Sigrist and D. F. Agterberg, Prog. Theor. Phys. **102**, 965 (1999).
[16] E. Babaev, Phys. Rev. Lett. **89**, 067001 (2002).
[17] E. Babaev, L. D. Faddeev, and A. J. Niemi, Phys. Rev. B **65**, 100512 (2002).
[18] R. Kato, Y. Enomoto, and S. Maekawa, Physica C **227**, 387 (1994).
[19] R. Kato, Y. Enomoto, and S. Maekawa, Phys. Rev. B **47**, 8016 (1993).
[20] M. Machida and H. Kaburaki, Phys. Rev. Lett. **71**, 3206 (1993).
[21] M. Ichioka, N. Nakai, and K. Machida, J. Phys. Soc. Jpn. **72**, 1322 (2003).
[22] See EPAPS Document No. E-PRBMDO-70-R04434 for movie version of Figs. 2 and 3. A direct link to this document may be found in the online article's HTML reference section. The document may also be reached via the EPAPS homepage (http://www.aip.org/pubservs/epaps.html) or from ftp.aip.org in the directory /epaps/. See the EPAPS homepage for more information.